MOI OF PATTERN FORMATION IN THE VORTEX LANDSCAPE

Rinke J. Wijngaarden, C.M. Aegerter, M.S. Welling and K. Heeck
Faculty of Sciences, Division of Physics and Astronomy, Vrije Universiteit,
De Boelelaan 1081, 1081 HV Amsterdam, The Netherlands
RW@NAT.VU.NL

Abstract Due to the occurence of punctuations or avalanches, flux penetration in superconductors is not the smooth process that is described in many textbooks. We investigate the relationship between spatial fluctuations of the vortex density map and vortex avalanches. For the experiment, we use a magneto-optical image lock-in amplifier. The optimization of this apparatus, in particular with respect to noise reduction is discussed.

Keywords: polarimeter, magneto-optics, superconductivity, roughening, avalanches

1. Introduction

Flux penetration in superconductors is an inherently unstable process, as is clear from the quenching of superconducting magnets. The magneto-optical technique enables a detailed study of the instabilities involved. It turns out that even the Bean state is not completely geometry-determined, but often displays roughening behavior[1], where an initially straight interface (e.g. between Meissner and Shubnikov phases) becomes increasingly 'wiggly'.

We use a specially developed magneto-optical image lock-in amplifier to accurately measure the local magnetic field above thin film superconductors. If the local field H_z at position (x, y) in the sample is plotted along the $z-$axis, the resulting 3-dimensional surface is not smooth, but reminiscent of the somewhat irregular surface of a granular pile (such as a heap of sand). From a roughness analysis[2] the growth exponent β and roughness exponent α for that surface may be found.

A close look at the evolution of the surface $H_z(x, y)$ reveals that its change as a function of the applied field is not continuous, but that the surface evolves by small and large sudden punctuations or avalanches.

These avalanches are characterized by their size distribution function (with exponent τ) and self-similar topology (with fractal dimensions d_B and D).

In the present work we determine the exponents and dimensions mentioned above for flux penetration in thin-film $YBa_2Cu_3O_7$ superconductors and check experimentally scaling relations for self-organized criticality (SOC)[3].

In section 2 we discuss the experimental apparatus in some detail in view of the emphasis of this workshop. In particular we discuss the effect of (shot)noise in the camera on the determination of the local magnetic field as well as the effect of various possible imperfections in the measurement procedure.

In section 3 the experimental procedure is discussed. In section 4 the method of analysis is given and our results are presented. The paper ends with a brief discussion of our findings.

2. Experimental apparatus

We study roughening and vortex avalanches in 80 nm thick $YBa_2Cu_3O_7$ films deposited on $NdGaO_3$ substrates by pulsed laser deposition[4]. Early results on the roughening behavior of the flux front were reported by Surdeanu et al.[1].

To local vortex density in the type-II $YBa_2Cu_3O_7$ superconductor is determined from the z-component of the magnetic field, H_z, immediately above the sample by a magneto-optical technique. We use the Faraday effect in a sensitive garnet film with in-plane anisotropy, that is coated with a mirror layer. The mirror is in direct contact with the $YBa_2Cu_3O_7$ sample, while the substrates of sample and indicator face outwards. The local H_z-field is determined from the angle of rotation in the garnet film by a polarization microscope set-up.

To be able to measure at high magnetic fields and at arbitrary temperatures in the range $2 - 300$ K, we use a commercial Oxford instruments magnet system with a specially designed microscope insert.

The insert, made of phosphor bronze, is shown in detail in figure 1. The sample assembly (i.e. sample and indicator mounted together on a dove-tail base plate) is placed in the dove-tail connection indicated in the figure. To be able to view with the microscope various parts of the sample, the holder has x and y motion. The cylindrical parts x, y screw into the body b. If they are rotated, their lower conical parts push on cantilevers c (only one is visible) that move the spring-loaded xy-table XY in respectively the x and y direction. To reflect the Faraday-rotated light exactly straight upwards into the microscope, the body b (which

is spring-loaded against the plate r by the spring S and rests on the ball B) can be tilted by the screws ϕ and ψ, which push against the reference plate r. To reduce the undesirable contrast between different domains in the indicator film, the magnetization vectors of the domains must be oriented correctly with respect to the polarization vector of the incident light. This can be done by rotating the dove-tailed sample holder with respect to the xy-table using screw θ. This rotating part and the xy-table are moving on 1 mm diameter sapphire ball-bearings. For coarse focussing, the whole assembly shown in the right-hand part of figure 1 can be moved in the z-direction, i.e. along the optical axis of the microscope, by rotating the screw z, that is screwing in block f and is fixed in a bearing with respect to the reference plate r. Block f can be fixed with respect to the cryostat by spring loaded pins p, which can be retracted for removal of the insert from the cryostat by a screw not shown. The whole assembly of figure 1 is at the end of a 70 cm long insert such that the sample is at the magnet centre-line position.

All controls and screws are connected to long thin rods (see figure 2c) that run to the insert main body (figure 2b) where two 45° rotary joints (knees) are used to connect to commercial rotary feedthroughs thus allowing to make all adjustments from the outside while the sample assembly is at low temperature. The whole magnet system is shown in

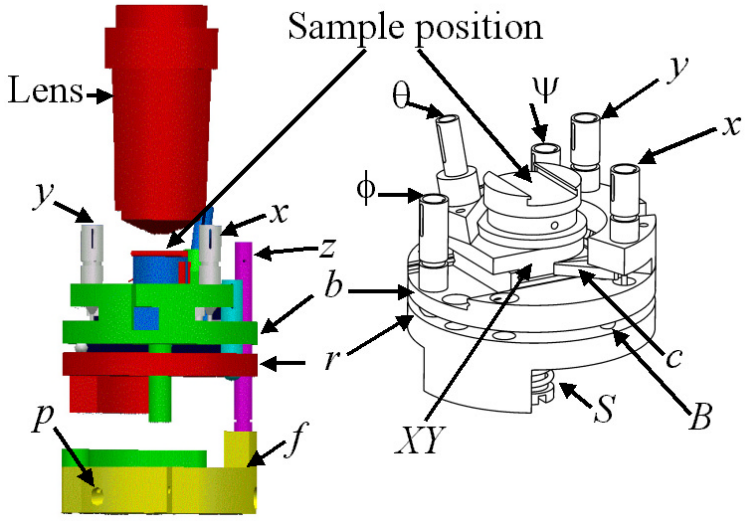

Figure 1. Detail of the insert showing the mechanism allowing x, y, z and θ, ϕ, ψ adjustments. For explanation see text.

figure 2a. The camera, indicated by C, is immediately above the main body of the insert.

In conventional magneto-optics, the local magnetic field is visualized by polarization microscopy as an image intensity I related to the Faraday angle ϕ by Malus law $I = L\sin^2\phi$, where L is the intensity of the illumination source. This method has several disadvantages: (i) one cannot determine the sign of ϕ (and hence of H_z since $\phi \sim H_z$) (ii) for ϕ close to zero the sensitivity is very low and (iii) one needs to know L as a function of position in the sample. To some extent the first two problems are alleviated by the well-known trick to slightly uncross the polarizer and analyzer. We have developed[5] an extension of that idea, which we call magneto-optic image lock-in amplifier (MO-ILIA). The main idea is to modulate the relative orientation of polarizer and analyzer. If the deviation from crossed position is α, then the intensity after the analyzer is given by $I = K + L\sin^2(\phi + \alpha)$, where we have added an offset-intensity K, which may be due to stray-light, imperfect extinction ratio of the polarizers or camera read-out offset. For small angles α and ϕ (in practice always true) the outcoming intensity may be approximated by $I = K + L(\phi + \alpha)^2$. By measuring intensities $\{I_+, I_0, I_-\}$ for three different values $\alpha = \{+\alpha_0, 0, -\alpha_0\}$, the unknowns ϕ, K and L are

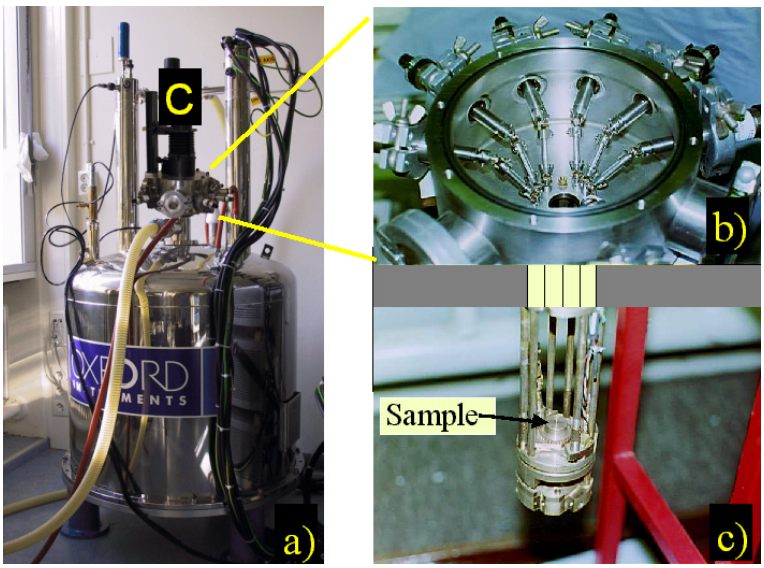

Figure 2. (a) Overall view of the cryostat with magnet and the insert. The camera position is indicated by C. (b) Main body of the insert (without top cover) showing the 45° joints and rotary feedtroughs. (c) Lower part of the insert containing the mechanism shown in figure 1.

determined. In particular:

$$\phi = \frac{I_+ - I_-}{4\alpha_0 L} \tag{1}$$

$$L = \frac{I_+ + I_- - 2I_0}{2\alpha_0^2} \tag{2}$$

The calculation of ϕ and L is carried out for each pixel in the image separately, either by special hardware in real-time at video rate[5] or at slower speed by software. The great advantage is a reliable determination of ϕ (including its sign) and hence of H_z irrespective of stray-light, uneven illumination etc. The price to pay is an increase in noise in the measurement of ϕ. Due to the term $(I_+ - I_-)$ in eq. 1, the absolute amount of noise will increase by about a factor $\sqrt{2}$. If K is large (e.g. due to poor extinction ratio of the polarizers), the *relative* noise is increased very much due to the shot-noise nature of light intensities (noise $\sim \sqrt{I}$). In that case the intensities I_+ and I_- are large and hence the noise $\sqrt{I_\pm}$ in these images is also large, while the intensity modulation $(I_+ - I_-)$ due to the rotation in the sample is small, leading to a large relative noise $\sqrt{2I_\pm}/\ (I_+ - I_-)$. Clearly, even with our modulation scheme, low K and good polarizers are essential. Potentially another source of noise is L, which enters in the denominator of eq. 1. This is especially worrying since L can become close to zero in the presence of noise. For this reason, one may prefer[6] to use only $\phi \sim (I_+ - I_-)$ hence omitting the normalization for uniform illumination. However, we prefer to include the normalization[5]. Since the sample illumination is mainly uneven in space and varies only very slowly in time (due to lamp ageing e.g.), it is justified to reduce the noise caused by L to negligible amount by averaging L in time. Typically, the running-averaging $L_{av} = kL_{in} + (1-k)\,L_{av}$ is calculated over $N = 100$ images ($k = 0.01$), while taking care that before real data are taken the running average is steady. The convergence at the start of the experiment can be greatly sped up by the following recursion, based on the recursive least squares algorithm [7]:

$$k_{n+1} = \frac{k_n}{e^{-1/N} + k_n} \tag{3}$$

that starts with $k_0 = 1$ and then slowly converges to $k_\infty = 1 - e^{-1/N}$ (e.g. for $N = 100$ to $k \simeq 0.01$).

Noise is also increased by imperfect crossing of the polarizer and analyzer. A crossing-error angle δ is equivalent to an extra rotation in the

sample and may be incorporated in the formulae above by the replacement $\phi \rightarrow \phi+\delta$. Due to the resulting larger intensities I (if α and ϕ and δ are in the same direction), the noise $\sqrt{I}$ increases, while the sample rotation is unmodified.

For the modulation of the angle α, we use a glass (Schott SF 59) rod with a large Faraday effect in a copper solenoid magnet optimized for field homogeneity and connected to electronics that enables switching the current in a few ms (in the video blanking time). We choose this glass because of its low absorption compared to garnet films. If intensity is not at stake, the much more compact construction of Indenbom[6] may be preferable.

If the modulation is done manually, there is always a risk of using a slightly asymmetric modulation $\alpha = \{+\alpha_0 + \varepsilon, 0, -\alpha_0\}$ instead of $\alpha = \{+\alpha_0, 0, -\alpha_0\}$, resulting in a calculated ϕ_{calc} given by

$$\phi_{calc} = \phi + \frac{\phi\varepsilon}{2\alpha_0} + \frac{\varepsilon}{2}$$

which leads to a change in ϕ by a factor $(1 + \varepsilon/2\alpha_0)$, which for typical values should be smaller than 10%, and to an offset $\frac{\varepsilon}{2}$, which is particularly significant at positions in the image where the rotation angle ϕ is close to zero.

To finish this discussion of the effects of noise with a quantitative statement, we calculate the effect of shot-noise in the images for the case of perfect symmetric modulation of α. If the calculation in eq. 2 is done with averaging over N images, then a simple error propagation analysis[8] yields a noise amplitude $\delta\phi$ in the calculated Faraday angle ϕ given by:

$$\delta\phi = \frac{1}{\sqrt{8L}}\sqrt{1 + \frac{K}{L\alpha_0^2} + \left(1 + \frac{4}{N} + \frac{12}{N}\frac{K}{L\alpha_0^2}\right)\frac{\phi^2}{\alpha_0^2} + \frac{12}{N}\frac{\phi^4}{\alpha_0^4}} \qquad (4)$$

For $N \longrightarrow \infty$ this reduces to

$$\delta\phi = \frac{1}{\sqrt{8L}}\sqrt{1 + \frac{K}{L\alpha_0^2} + \left(\frac{\phi}{\alpha_0}\right)^2} \qquad (5)$$

For $N = 100$ the difference in $\delta\phi$ calculated by eq. 5 or eq. 4 is less than 1%. Clearly the noise can be greatly reduced by increasing the illumination intensity L. Unfortunately, L cannot be increased at will, since the well-capacity of the CCD-camera limits the maximum number of photons that can be registered. The optimum is obtained by setting the illumination intensity L before the start of the experiment as high as possible but such that the saturation intensity of the camera $I_{\max}$

is just not reached for any local magnetic field and for any modulation angle α to be used during the experiment. Since $I = K + L\left(\alpha + \phi\right)^2$, this implies that one chooses the illumination intensity L such that

$$L\left(\alpha_0 + |\phi_{\max}|\right)^2 = I_{\max} - K = C \tag{6}$$

where we introduce for brevity the new constant C. Under this optimal condition, the noise is given by

$$\delta\phi = \frac{1}{\sqrt{8C}}\sqrt{\frac{\left(\alpha_0+\phi\right)^4}{\alpha_0^2}\frac{K}{C} + \left(\alpha_0+\phi\right)^2 + \frac{\phi^2\left(\alpha_0+\phi\right)^2}{\alpha_0^2}} \tag{7}$$

from which one easily calculates that the maximum of the signal to noise ratio $S/N = \phi/\delta\phi$ is obtained for $\alpha_0 = \phi_{\max}$.

3. Experimental procedure

After a cool down in zero field (ZFC), an external magnetic field is applied perpendicular to the sample surface. We measure the local H_z-field directly above the sample with the MO-ILIA as described above. Since each vortex carries one flux quantum $\Phi_0 = \frac{h}{2e}$ and since at the surface the vortices are perpendicular to the surface, the field H_z is a direct measure of the vortex density. A typical plot of this vortex density as a function of position in the sample is shown in figure 3; the spatial resolution is such that 1 pixel corresponds to 1.4 μm.

The similarity of the figure with a heap of sand is striking. In five experiments[9] at 4.2 K, each time after ZFC, the magnetic field is increased from 0 mT to 17 mT with a sweep rate of 1 mT/s in 50 μT steps. At every step, the sample is relaxed for 10 seconds after which an image is acquired. Below we analyze the roughness of the 2-dimension surfaces of these 'piles' and find the avalanches that create the surface roughness. Then we relate the statistical properties of the avalanches to those of the surface.

4. Analysis and discussion

A rough interface, like the one shown in figure 3, can be characterized by the properties of its root-mean-squared width w. In the initial state of formation of the surface, this width grows with time t as a power law: $w \sim t^{\beta}$ where β is called the growth exponent. In later stages, this growth is limited at a value w_{sat} by the system size L, where $w_{sat} \sim L^{\alpha}$ is found. A more accurate determination of the exponents is obtained

by using instead of w the two point correlation function:

$$C(\vec{x},t) = \left(\langle (b(\vec{\xi},\tau) - b(\vec{x}+\vec{\xi},t+\tau))^2 \rangle_{\vec{\xi},\tau}\right)^{1/2} \tag{8}$$

which has[2] similar scaling behavior: $C(|\vec{x}|,0) \propto |\vec{x}|^{\alpha}$ and $C(0,t) \propto t^{\beta}$. Plots of $C(|\vec{x}|,0)$ and $C(0,t)$ for the five experiments[8] show nice power law scaling behavior. From these plots we find $\alpha = 0.79(10)$ and $\beta = 0.60(10)$. The roughness exponent α is large and close to that found for certain mountain ranges[10], pointing to a large influence of static disorder (pin centers) in the superconductor on the flux penetration process.

If two interfaces (such as shown in figure 3) at consecutive fields are subtracted, the difference is partially due to the change in externally applied magnetic field and partially due to fluctuations caused by the flux penetration process. To study the latter, we subtract the change in external field from the difference between two consecutive images. The resulting image Δ is a map of redistributions of flux due to avalanches. If the penetration process was completely homogeneous, Δ would be indentical to zero everywhere. By contrast, in our experiment Δ is negative where an avalanche has removed vortices and positive where an avalanches has deposited vortices. The sum over the whole image of *the absolute value* of all values in Δ hence yields twice the total flux in an avalanche. Clearly, from Δ one may also determine the avalanche shape, its volume fractal dimension D and its surface fractal dimension d_B (i.e.

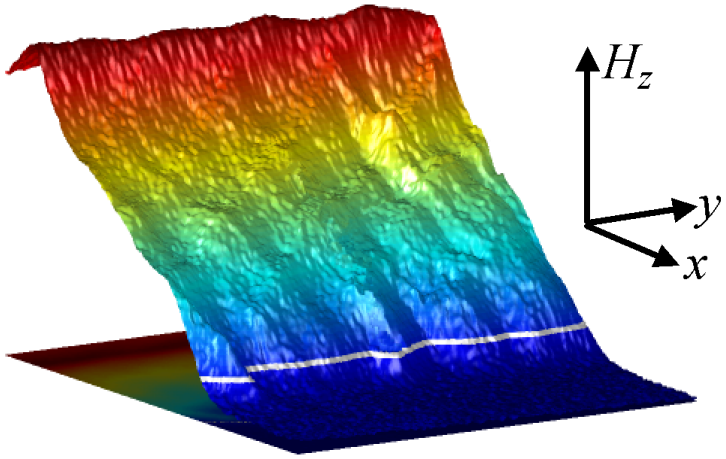

Figure 3. Local magnetic field H_z (vertical) as a function of position in the sample (horizontal plane) at 15 mT external field after zero field cooling at 4.2 K. The edge of the sample is at the position of the top of the ridge.

for the projection of the avalanche shape on a plane corresponding to the pile average surface).

In figure 4, the probabilities $P(s, L)$ for finding an avalanche of size s in a sample of linear size L are plotted. In reality we do not use different sample sizes L; instead, we analyze subsets of our sample with size L. Note that the straight line in figure 4 indicates that the probability $P(s, L)$ scales with the avalanche size as a power law: $P(s, L) \sim s^{-\tau}$, which is a hall-mark for self-organized criticality (SOC)[3]. The deviations at large avalanche size are due to the fact that an avalanche cannot span more than the whole system. Hence the relation $P(s, L) \sim s^{-\tau}$ has a system size dependent cut-off as clearly seen in the figure. It is remarkable that this cut-off can be used[11] to make a more stringent test for SOC: it is required by SOC theory that the cut-off size scales as L^D (so-called finite-size scaling). In the inset of figure 4, the results are rescaled horizontally with a factor L^D and vertically with s^τ to take out the power law. Both D and τ were used as fitting parameters. Clearly a nice collapse of data for the various system sizes is obtained, giving more strength to the idea that our system is SOC. Using the results from the roughness analysis described above, even more tests for SOC can be made: it is predicted[11],[12] that $D = d_B + \alpha$ and

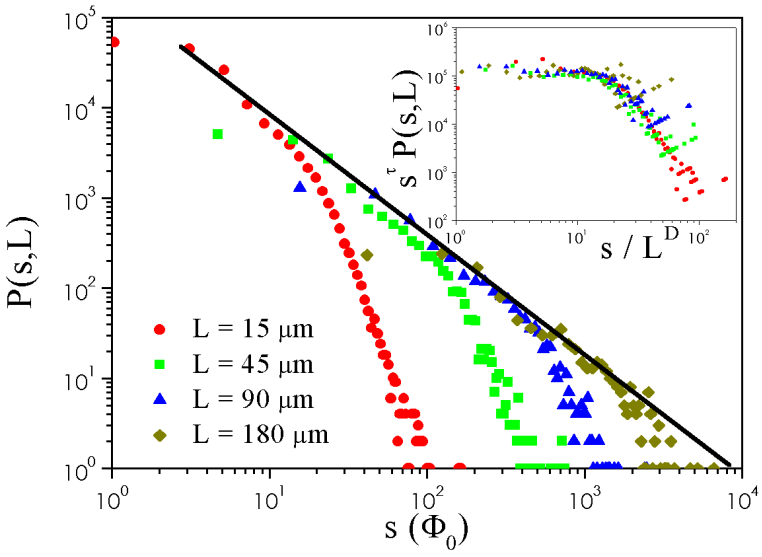

Figure 4. Probablility distribution $P(s, L)$ for avalaches of size s in a system of linear dimension L. The cut-off is due to avalanches reaching the system size. The inset shows the results of finite size scaling with $D = 1.89(3)$ and $\tau = 1.29(2)$. Note the nice data collapse.

that $\alpha/\beta = D\,(2-\tau)$. Using these relations and our experimental values $D = 1.89(3)$, $d_B = 1.18(5)$ and $\tau = 1.29(2)$, we find $\alpha = 0.71(6)$ and $\beta = 0.53(6)$ while from the roughness analysis above we have $\alpha = 0.79(10)$ and $\beta = 0.60(10)$. Clearly, within experimental accuracy, the SOC relations $D = d_B + \alpha$ and $\alpha/\beta = D\,(2-\tau)$ are satisfied. Although further experimental tests (if possible with higher accuracy) are certainly desirable, we conclude in view of (i) the experimental verification of these scaling relations (ii) the power law distribution of avalanche sizes and (iii) the finite size scaling, that there is rather strong experimental evidence for SOC in the vortex matter of our sample.

Acknowledgments

We thank J. Rector and B. Dam for providing the samples. This work was supported by FOM (Stichting voor Fundamenteel Onderzoek der Materie), which is financially supported by NWO (Nederlandse Organisatie voor Wetenschappelijk Onderzoek). We acknowledge the VORTEX program of the European Science Foundation for support.

References

[1] R.Surdeanu, R.J. Wijngaarden, E. Visser, B. Dam, J. Rector and R. Griessen, Phys.Rev.Lett. **83**, 2054 (1999)

[2] A.-L. Barabási and H. E. Stanley, Fractal Concepts in Surface Growth, Cambridge University Press (Cambridge, 1995).

[3] P.Bak, How Nature Works, Spinger Verlag (New York, 1996)

[4] J. M. Huijbregtse, B. Dam, J. H. Rector, and R. Griessen, J. Appl. Phys. **86**, 6528 (1999).

[5] R. J. Wijngaarden, K. Heeck, M. Welling, R. Limburg, M. Pannetier, K. van Zetten, V.L.G. Roorda, A.R. Voorwinden, Rev. Sci. Instrum. **72**, 2661 (2001).

[6] See the contribution by M.V. Indenbom in this volume.

[7] B. Friedlander, *Adaptive algorithms for finite impulse response filters* in *Adaptive filters*, C.F.N. Cowan and P.M. Grant, eds., Pretice Hall (Engelwood Cliffs NJ, 1985)

[8] M.S. Welling, C.M. Aegerter and R.J. Wijngaarden, to be published

[9] M.S. Welling, C.M. Aegerter and R.J. Wijngaarden, Europhysics Lett. **61**, 473 (2003)

[10] A. Czirók, E. Somfai, and T. Vicsek, Phys. Rev. Lett. **71**, 2154 (1993).

[11] M. Paczuski, S. Maslov and P. Bak, Phys. Rev. E **53**, 414 (1996)

[12] C. M. Aegerter, R. Günther, and R. J. Wijngaarden, Phys. Rev. E **67**, 051306 (2003)